Detecting causal interdependence in simulated neural signals based on pairwise and multivariate analysis

Chufeng Yang , Régine Le Bouquin Jeannes * , Gérard Faucon , Fabrice Wendling

LTSI, Laboratoire Traitement du Signal et de l'Image INSERM : U642 , Université de Rennes I , FR

* Correspondence should be adressed to: Régine Le Bouquin Jeannes <regine.lebouquin@univ-rennes1.fr >

Abstract

Our objective is to analyze EEG signals recorded with depth electrodes during seizures in patients with drug-resistant epilepsy. Usually, different phases are observed during the seizure process, including a fast onset activity (FOA). We aim to determine how cerebral structures get involved during this FOA, in particular whether some structure can "drive" some other structures. This paper focuses on a linear Granger causality based measure to detect causal relation of interdependence in multivariate signals generated by a physiology-based model of coupled neuronal populations. When coupling between signals exists, statistical analysis supports the relevance of this index for characterizing the information flow and its direction among neuronal populations.

Introduction

Epilepsy is a neurological disorder characterized by repetitive seizures. In 30% of the cases, seizures remain drug-resistant and considerably affect all aspects of the patient's life [1]. Drug-resistant epilepsies are often partial, with an epileptogenic zone (EZ) located in a relatively circumscribed brain area. For these partial epilepsies, surgical treatment can be considered. The difficulty that arises is then to determine the organization of the EZ and, thus, the areas that should be removed in order to suppress seizures. In some patients, the pre-surgical evaluation may include recording of intracerebral electroencephalographic (iEEG) signals using depth electrodes. The analysis of such signals remains a difficult task aimed at determining which sites of the brain belong to the EZ, prior to surgery. In this context, signal processing techniques can provide some quantitative information that cannot be easily obtained by visual analysis. This is typically the case for correlation (wide-sense) measures that proved useful for assessment of functional couplings between distant brain sites [2]. In this paper, we present some evaluation results about a method allowing for determination of causality relationships among neuronal ensembles from signals produced by these ensembles (typically local field potentials or iEEG signals). The concept of causality between time series was first introduced by Wiener [3] in 1956, then formulated by Granger [4] and known as Granger Causality Index (GCI). Granger causality is a statistical concept of causality that is based on prediction and has been widely used in economics since the 1960s. According to Granger causality, if a signal x_1 "causes" a signal x_2, then past values of x_1 should contain information that helps predict x_2 above and beyond the information contained in past values of x_2 alone. If GCI is an effective tool to describe causal interactions between signals, it is only within the last few years that applications in neuroscience have become popular [5]–[7]. In this paper, the method is evaluated on signals simulated from physiology-based model of coupled neuronal populations in which causality relationships can be controlled. The key features of this model are two-fold. First, it generates signals for which properties are similar to those of real signals observed at the onset of epileptic seizures. Second, it provides a "ground truth" about the degree and direction of couplings between populations of neurons, which is hardly accessible on real data.

Material and Methods

Linear Granger Causality Index (LGCI)

Granger causality is normally tested in the context of linear regression models. Let $x_1,\ldots, x_Q$ be Q zero-mean signals whose discrete-time observations are noted $x_1(t), x_2(t),\ldots, x_Q(t)$, $t = 1,2,\ldots,T$, where T is the signal length. If we model the observations by a multivariate autoregressive (AR) model of order m , we write

$$\begin{bmatrix} x_1(t) \\ \vdots \\ x_Q(t) \end{bmatrix} = \sum_{k=1}^{M} A_k \begin{bmatrix} x_1(t-k) \\ \vdots \\ x_Q(t-k) \end{bmatrix} + \begin{bmatrix} w_1(t) \\ \vdots \\ w_Q(t) \end{bmatrix}$$

where each signal depends not only on its own past but also on the past of the other signals. $w_i(t)$, $i = 1, 2,\ldots, Q$, are white Gaussian noises, and

$$A_k = \begin{bmatrix} \alpha_{1.1}(k) & \alpha_{1.2}(k) & \cdots & \cdots & \alpha_{1.Q}(k) \\ \vdots & \vdots & \vdots & \vdots & \vdots \\ \vdots & \vdots & \vdots & \alpha_{i.j}(k) & \vdots \\ \vdots & \vdots & \vdots & \vdots & \vdots \\ \alpha_{Q.1}(k) & \cdots & \cdots & \cdots & \alpha_{Q.Q}(k) \end{bmatrix}.$$

The coefficient $\alpha_{i.j}(k)$ evaluates the linear interaction of $x_j(t-k)$ on $x_i(t)$, whatever i , j . These coefficients are estimated by solving Yule–Walker equations.

Let us begin with the case of two signals by studying the causality $x_1 \rightarrow x_2$. From an univariate model, the quality of the representation of x_2 may be evaluated from the variance of the prediction error $\Gamma_{x_2|x_2^-}$, where x_2^- symbolizes x_2 past. Using a bivariate model, the variance of the prediction error becomes $\Gamma_{x_2|x_2^-,x_1^-}$. If x_1 causes x_2 in the Granger sense, then $\Gamma_{x_2|x_2^-,x_1^-}$ is smaller than $\Gamma_{x_2|x_2^-}$. Considering pairwise analysis, the level of LGCI from x_1 to x_2 is then evaluated by

$$\mathrm{LGCI}_{12} - \mathrm{P} = \ln \frac{\Gamma_{x_2|x_2^-}}{\Gamma_{x_2|x_2^-,x_1^-}}.$$

Reciprocally, the LGCI from x_2 to x_1 can be evaluated.

In the case of multiple signals, we can analyze independently each pair of signals as previously. However, pairwise analysis in this multivariate case cannot distinguish between direct and indirect coupling. In the multivariate case, to disambiguate such cases, direct causality from x_i to x_j conditionally to other signals is noted LGCI_{ij}-M and defined by (4) where the numerator is the variance of the prediction error of x_j by taking all signals into account except x_i

$$\mathrm{LGCI}_{ij} - \mathrm{M} = \ln \frac{\Gamma_{x_j|x_1^- \cdots x_{i-1}^- x_{i+1}^- \cdots x_Q^-}}{\Gamma_{x_j|x_1^- \cdots x_Q^-}}.$$

Model of iEEG Signals Generation

We used a physiology-based model to simulate the field activity of distant - and possibly coupled - neuronal populations. Each population generates a local activity that can be considered as an iEEG signal if one does not consider the source-electrode quasi-static transfer function. Readers may refer to [8], [9] for more information. In the model, each population contains three subpopulations of neurons that mutually interact via excitatory or inhibitory feedback: main pyramidal cells and two types of local interneurons. Since pyramidal cells are excitatory neurons that project their axons to other areas of the brain, the model accounts for this organization by using the average pulse density of action potentials from the main cells of one population i as an excitatory input to another population j . In addition, this connection from population i to j is characterized by parameter K^{ij} which represents the degree of coupling associated with this connection. Appropriate setting of parameters K^{ij} allows for building systems where the neuronal populations are unidirectionally or bidirectionally coupled. Other parameters include excitatory and inhibitory gains in feedback loops as well as average number of synaptic contacts between subpopulations. These parameters are adjusted to control the intrinsic activity of each population (normal background versus epileptic activity).

Simulated Signals

The model described above was used to simulate long duration signals (400 s) for a fixed connectivity pattern among neuronal populations, as illustrated in Fig. 1A and Fig. 1B . Sampling rate was equal to 256 Hz. Model parameters were such that: (i) a fast quasi-sinusoidal (25 Hz, Fig. 1C) activity (similar to that observed at seizure onset) was generated by the three populations when they were unidirectionally coupled (1→2→3) and (ii) this fast onset activity was only generated by population 1 when they were uncoupled. In this second situation, populations 2 and 3 generated normal background activity (not shown).

This scenario ensured that the epileptic activity present in populations 2 and 3 was caused by that of population 1. Another key aspect is that the spectral features of output signals are very close under the “coupled” condition. In addition, some jitter might be observed between simulated time series (Fig. 1B) as also observed in real situations, at seizure onset.

Results

In this section, we present results on (i) LGCI in presence or absence of coupling, (ii) the influence of coupling strength. For the experiments, when there is a coupling between observations, the coupling coefficients are chosen identical, i.e. $K^{12} = K^{23} = K$. Model order m is estimated by minimizing the Akaike's information criterion (AIC) on each frame.

Detection of Information Flow

Firstly, we estimate LGCI considering pairwise analysis of signals (LGCI-P) and multivariate analysis (LGCI-M). The indices depend on the coupling and on the signals under study. LGCI is performed on 1024-point adjacent frames corresponding to sequences of 4s time duration, which is suitable for real signals (estimating changes below this value appears more difficult). For our simulated signals, we obtain 100 values of indices. Table I reports the averaged indices for K = 0 and K = 1500. For K = 0, on the one hand, the averaged LGCI-P are similar (about 0.005) and, on the other hand, the averaged LGCI-M are also similar (about 0.003). Now, let us consider a coupling between signals using K = 1500. As expected, LGCI from x_1 to x_2 and from x_2 to x_3 increase, both in pairwise and multivariate analysis. For each index, the variation (without coupling vs with coupling) is comparable using LGCI-P or LGCI-M (around 0.015 for $LGCI_{12}$, and around 0.005 for $LGCI_{23}$). This finding means that detecting the flow $x_2 \rightarrow x_3$ is more difficult than detecting the flow $x_1 \rightarrow x_2$. As for the relation $x_1 \rightarrow x_3$, it is indirect and completely mediated by signal x_2. Consequently, when K = 1500, $LGCI_{13}$-M remains at a low value (0.0039 vs 0.0031) since it is based on a multivariate analysis. Fitting a two-dimensional AR model, the $LGCI_{13}$-P index, which should have risen, does not sufficiently increase to reveal an influence from x_1 to x_3. Let us note that all other indices, corresponding to the opposite directions $x_2 \rightarrow x_1$, $x_3 \rightarrow x_2$ and $x_3 \rightarrow x_1$, remain low and quite constant in both conditions and present a lower variation using multivariate analysis. According to these remarks, we displayed on Fig. 2 the time evolution of $LGCI_{12}$-M and $LGCI_{21}$-M, for K = 1500, showing that $LGCI_{12}$-M is generally greater than $LGCI_{21}$-M. To confirm these results, statistical significance has to be addressed.

Statistical analysis on LGCI-P and LGCI-M is summarized in Tables II and III . In these tables, the last column gives the value of the hypothesis test (a value of 1 indicates that the null-hypothesis is rejected) and the expected value according to our scenario is given into brackets. In Table II , we test whether LGCI computed from signal i to signal j is significantly different from LGCI computed from signal j to signal i using the Wilcoxon signed-rank test. The unidirectional information flow from signal 1 to signal 2 is obvious with a very low p -value for pairwise or multivariate analysis (lower than 1e-16). In the same way, we can conclude on the information flow from signal 2 to signal 3 with a p -value at least lower than 1e-3. For both indices, the only difference relies on the information flow from signal 1 to signal 3. For LGCI-M, the result is coherent: there is no direct relation between the two signals. As for LGCI-P, since signals are studied by pairs, we must find information flow from signal 1 to 3 but we can notice that the index fails in this case (h = 0).

The second test, presented in Table III , consists in pointing out the effective coupling between signals when the parameter K turns from 0 to 1500. Estimators are tested only for the real causal relations (either direct or indirect). It comes out that, in each case, using either LGCI-P or LGCI-M, the Mann-Whitney test reveals a coupling from signal 1 to signal 2, and from signal 2 to signal 3. As previously, the interaction from signal 1 to signal 3 cannot be put forward using LGCI-P, whereas it should be the case. On the other hand, LGCI-M does not reject the null-hypothesis since there is no direct relation between populations 1 and 3.

Variable Coupling

In this section, we study the significant influence of the coupling parameter K on LGCI in the vectorial case. Fig. 3 shows the evolution of $LGCI_{12}$-M, $LGCI_{23}$-M and $LGCI_{13}$-M, when K varies from 100 to 1500 by step of 100. $LGCI_{12}$-M and $LGCI_{23}$-M vary linearly with K (with a steeper slope for $LGCI_{12}$-M) while $LGCI_{13}$-M is quite stable. So, the directions $x_1 \rightarrow x_2$ and $x_2 \rightarrow x_3$ are easier to detect when K increases.

We first tested the significance of LGCI-M between populations 1 and 2 for a value of K different from 0. The value of h using the Wilcoxon test is plotted in Fig. 4 . For a p -value of 0.05, the test indicates a flow direction from population 1 to population 2 as soon as K reaches 500. When we test $LGCI_{12}$-M without and with coupling (K varying from 100 to 1500), the Mann-Whitney test indicates a significant difference at a p -value of 0.05, whatever the value of K , except K = 100 and K = 400. In the same way, significant causality has been tested between populations 2 and 3. Testing $LGCI_{23}$-M versus $LGCI_{32}$-M can be sometimes not significant at a level of 5%, even for K greater than 500. Now, testing $LGCI_{23}$-M with and without coupling yields a significant difference above K = 700.

Conclusion

This paper was aimed at better understanding how seizure activity arises from a model of three neuronal populations. The a priori knowledge of effective coupling allows us to evaluate the relevance of Granger causality indices. The results reported in this paper show that the method can reveal the underlying network organization in a difficult situation where time shifts between signals strongly vary in

time, as in the real case. Based on multivariate or pairwise analysis, direct causal relations are well detected for a sufficiently strong coupling whereas pairwise analysis may fail in detecting indirect relations. In a future work, according to the narrow-band characteristics of the signals, we plan to conduct statistical analysis in the frequency domain.

Ackowledgements:

This work was supported by China Scholarship Council (CSC) under Grant No. 2008609145.

References:

- 1 . Engel J , VanNess P , Rasmussen T , Ojemann L . Editor: Engel J . Outcome with respect to epileptic seizures . Surgical Treatment of the Epilepsies . 2 New York Raven Press ; 1993 ; 609 - 622
- 2 . Ansari-Asl K , Senhadji L , Bellanger JJ , Wendling F . Quantitative evaluation of linear and nonlinear methods characterizing interdependencies between brain signals . Phys Rev E Stat Nonlin Soft Matter Phys . 74 : (3 Pt 1) 031916 - 2006 ;
- 3 . Wiener N . Editor: Beckenbach EF . The theory of prediction . Modern Mathematics for Engineers . 1 : New York McGraw-Hill ; 1956 ; 125 - 139
- 4 . Granger CWJ . Investigating causal relations by econometric models and cross-spectral methods . Econometrica . 37 : 424 - 438 Aug 1969 ;
- 5 . Wang X , Chen Y , Bressler SL , Ding M . Granger causality between multiple interdependent neurobiological time series: Blockwise versus pairwise methods . Int J of Neural Systems . 17 : 71 - 78 2007 ;
- 6 . Kayser AS , Sun FT , D'Esposito M . A comparison of Granger causality and coherency in fMRI-based analysis of the motor system . Human Brain Mapping . 30 : 3475 - 3494 Nov 2009 ;
- 7 . Dauwels J , Vialatte F , Musha T , Cichocki A . A comparative study of synchrony measures for the early diagnosis of Alzheimer's disease based on EEG . NeuroImage . 49 : 668 - 693 Jun 2009 ;
- 8 . Wendling F , Bellanger JJ , Bartolomei F , Chauvel P . Relevance of nonlinear lumped-parameter models in the analysis of depth-EEG epileptic signals . Biological Cybernetics . 83 : 367 - 378 2000 ;
- 9 . Wendling F , Hernandez A , Bellanger JJ , Chauvel P , Bartolomei F . Interictal to ictal transition in human temporal lobe epilepsy: insights from a computational model of intracerebral EEG . J Clin Neurophysiol . 22 : 343 - 356 2005 ;

Fig. 1

Simulated signals. A. Considered scenario for connectivity among neuronal populations. Epileptic activity in population 2 (resp. 3) is caused by excitatory drive from population 1 (resp. 2). B. An example of output signals when populations are coupled. Time delays are not constant over time. C. Power spectral densities (PSD) of the signals are similar and match those observed in depth-EEG signals at the onset of seizures.

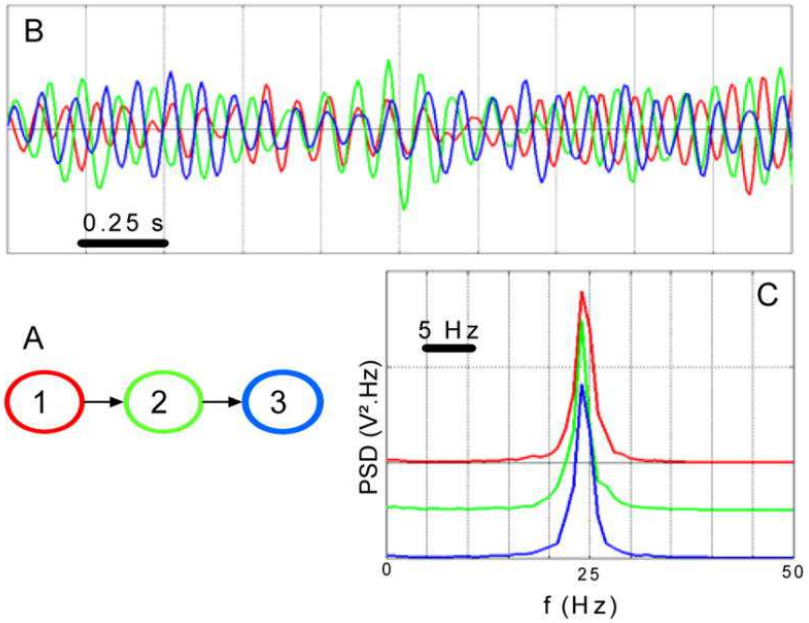

Fig. 2

$LGCI_{12}$ -M (K = 1500) (solid line) versus $LGCI_{21}$ -M (K = 1500) (dotted line).

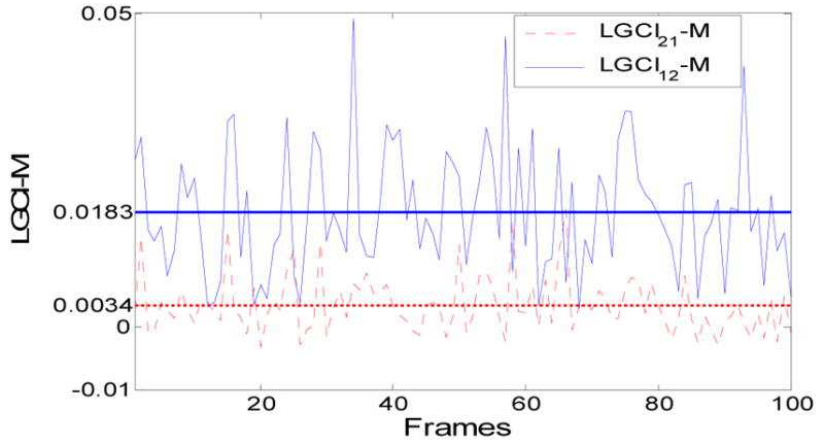

Fig. 3

LGCI-M with K varying from 100 to 1500.

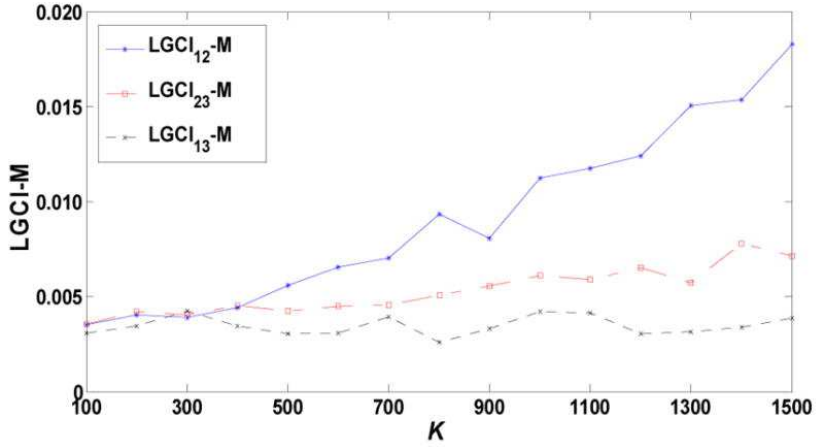

Fig. 4

$LGCI_{12}$ -M (K ≠0) versus $LGCI_{21}$ -M (K ≠0) (solid line) and $LGCI_{12}$ -M (K ≠0) versus $LGCI_{12}$ -M (K = 0) (dotted line) with K varying from 100 to 1500.

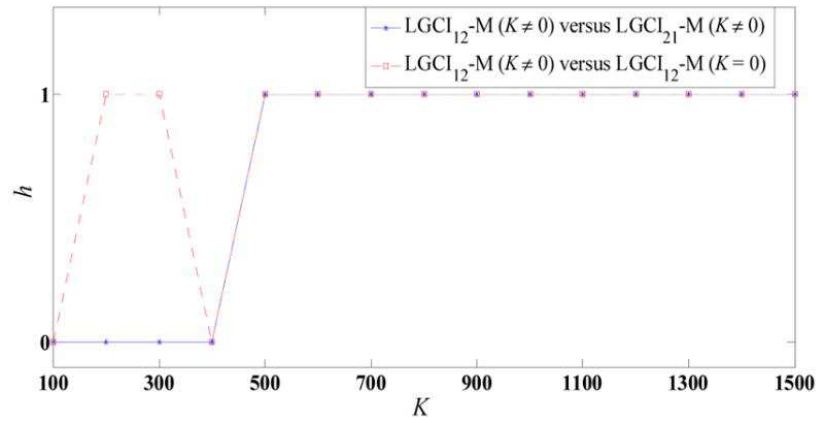

TABLE I

Results on LGCI-P and LGCI-M

LGCI-P				
K =0	$x_i \rightarrow x_j$	i = 1	i = 2	i = 3
	j = 1	-	0.0054	0.0048
	j = 2	0.0055	-	0.0046
	j = 3	0.0052	0.0047	-
K =1500	$x_i \rightarrow x_j$	i = 1	i = 2	i = 3
	j = 1	-	0.0064	0.0058
	j = 2	0.0209	-	0.0062
	j = 3	0.0059	0.0107	-
LGCI-M				
K =0	$x_i \rightarrow x_j$	i = 1	i = 2	i = 3
	j = 1	-	0.0034	0.0031
	j = 2	0.0032	-	0.0029
	j = 3	0.0031	0.0031	-
K =1500	$x_i \rightarrow x_j$	i = 1	i = 2	i = 3
	j = 1	-	0.0034	0.0036
	j = 2	0.0183	-	0.0046
	j = 3	0.0039	0.0071	-

TABLE II

Wilcoxon Test on LGCI-P and LGCI-M

LGCI-P (K = 1500)		
	p	**h , [expected value]**
$x_1 \rightarrow x_2$ vs $x_2 \rightarrow x_1$	6.7292e-017	1, [1]
$x_1 \rightarrow x_3$ vs $x_3 \rightarrow x_1$	0.8635	0, [1]
$x_2 \rightarrow x_3$ vs $x_3 \rightarrow x_2$	5.3566e-007	1, [1]
LGCI-M (K = 1500)		
	p	h , [expected value]
$x_1 \rightarrow x_2$ vs $x_2 \rightarrow x_1$	3.6417e-017	1, [1]
$x_1 \rightarrow x_3$ vs $x_3 \rightarrow x_1$	0.7859	0, [0]
$x_2 \rightarrow x_3$ vs $x_3 \rightarrow x_2$	2.6778e-004	1, [1]

TABLE III

Mann-Whitney Test on LGCI-P and LGCI-M

LGCI-P (K = 1500 vs K = 0)		
	p	**h , [expected value]**
$x_1 \rightarrow x_2$	4.8567e-026	1, [1]
$x_1 \rightarrow x_3$	0.6451	0, [1]
$x_2 \rightarrow x_3$	7.2285e-010	1, [1]
LGCI-M (K = 1500 vs K = 0)		
	p	h , [expected value]
$x_1 \rightarrow x_2$	3.7870e-027	1, [1]
$x_1 \rightarrow x_3$	0.7222	0, [0]
$x_2 \rightarrow x_3$	4.5928e-006	1, [1]